

Interfaces and falling drops in a Hele-Shaw cell

J F Nye, H W Lean and A N Wright†

H H Wills Physics Laboratory, University of Bristol, Bristol BS8 1TL, UK

Received 12 December 1983, in final form 15 February 1984

Abstract A Hele-Shaw cell can be used to explore a variety of phenomena that involve surface tension and viscosity simultaneously. Being essentially two-dimensional the effects are easy to observe, and often simple to calculate apart from fine details. Waves growing exponentially on an unstable interface, and tear drops falling slowly down the cell, are interesting examples.

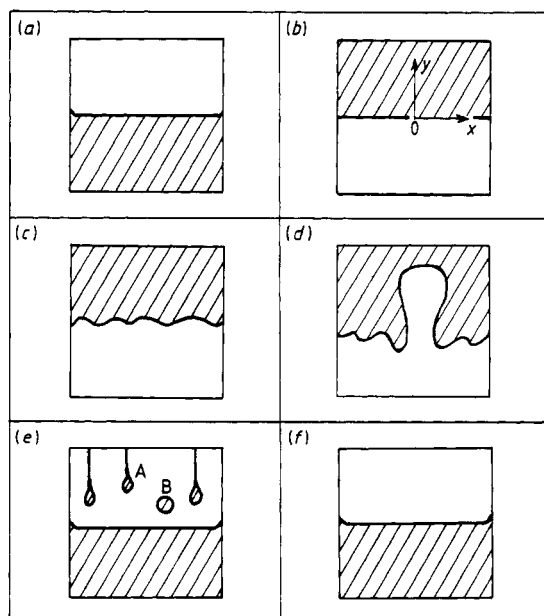
Résumé On peut utiliser une cellule de Hele-Shaw pour étudier un grand nombre de phénomènes qui font simultanément intervenir capillarité et viscosité. Les effets concernés, du fait de leur caractère bidimensionnel, sont faciles à observer et souvent simples à analyser mathématiquement, au moins en première approximation. Comme exemples particulièrement intéressants, on peut citer des ondes à croissance exponentielle à un interface instable et des larmes tombant lentement vers le bas de la cellule.

1. A simple experiment

Phenomena that involve the motion of the surface of a viscous liquid under the combined effects of surface tension and slow viscous flow are usually complicated by being three-dimensional. However, they can be made effectively two-dimensional, and hence more simply calculated and easier to observe, by the use of a Hele-Shaw cell. In this arrangement one views a layer of liquid sandwiched between two closely-spaced parallel flat plates, but in the present experiments, unlike the original ones (Hele-Shaw 1898a, b), the liquid only partially fills the space available to it, so that there is a free boundary.

A typical experiment, using oil between perspex plates, is shown in figure 1. The plates are vertical and in (a) the liquid fills the lower half of the cell, which is closed and approximately square. Because the oil wets the plates the oil-air interface is to a good approximation a half-cylinder of diameter equal to the gap between the plates; it appears simply as a very narrow horizontal straight band with sharp edges. The cell is now rapidly inverted. The new configuration (b) is in statical equilibrium (the cell being airtight), but the equilibrium is unstable. If the cell is wide enough, waves (c) develop at the interface, they grow unstably (d) and eventually (e) the liquid comes to rest again filling the

Figure 1 A closed vertical Hele-Shaw cell is half filled with liquid (a) and then inverted (b). Instabilities develop at the interface, (c) and (d); at a later stage drops fall from the upper edge (e) and eventually the original state is restored (f).



† Lean and Wright were undergraduates when this work was done and it formed part of their final year project.

lower half of the cell. The experiment (which takes about five minutes with the cell described in section 4) can now be repeated.

From the great variety of phenomena to be seen between stages (b) and (f) we have selected a few for detailed study. Just after inversion (c) the interface 'line' is quasi-sinusoidal with a measurable wavelength. In section 3 we calculate this wavelength and in section 4 we compare it with observations. At a later stage (e) drops of liquid (A) drift slowly downwards. At first they are connected by long tails to the thin horizontal thread of liquid that remains along the top of the cell. If its tail breaks before a drop reaches the main body of the liquid below it, the drop very rapidly becomes circular (B) and continues its descent. In sections 5 and 6 we calculate the shape and velocity of these tethered drops. On the assumption that the fluid velocity is uniform within a tethered drop the theoretical shape is universal, being independent of all constants. This is borne out by the observations to a good approximation. The observed rough uniformity in the spacing of these tethered drops can be explained (section 4) by considering their origin, for they arise from instabilities in the thin thread of liquid at the top of the cell.

The general behaviour between figure 1(b) and 1(e) is that areas of air ascend and areas of fluid descend, changing their shapes as they travel but at first preserving their topology. The topology changes in two distinct ways: when two fluid areas touch they immediately merge, but when two areas of air come into contact a liquid thread remains between them (as in the tether of a tethered drop) which lasts for a comparatively long time, thus temporarily preserving the topology. In the first case the cylindrical menisci meet with their concave sides facing one another, while in the second they meet convex to convex. In this second case a thin, narrow strip of film is formed perpendicular to the plane of the cell, which is a relatively stable arrangement. Eventually, however, drainage breaks the film, so that the thread suddenly disappears leaving a little liquid on each face of the cell.

By turning the cell in a vertical plane other interesting configurations may be seen evolving, and by tilting the cell out of the vertical plane the effect of gravity can be continuously varied; a variety of static interface shapes can then be made that are governed simply by gravity and surface tension (section 5). These include the two-dimensional analogue of the pendant drop shape much studied in three dimensions with cylindrical symmetry.

An attractive feature of this kind of experiment is the ease with which it can be done, once the cell is made, and the precision with which the interface can be observed. There is much more to see (and calculate) than can be described here. A version of the cell made with three plates and containing two independent coloured liquids was bought in the

USA by one of the authors as an 'executive toy'.

The traditional Hele-Shaw cell has arrangements for pumping the liquid between the plates and is used as an analogue for the three-dimensional flow of a fluid through a porous medium; in both cases the velocity is proportional to the gradient of a potential. In certain kinds of oil-well water is used to drive out the oil from the porous rock. When the velocity of extraction is too high long tongues of water, analogous to the tongues in figure 1(d), penetrate the oil and it emerges from the well mixed with water. Saffman and Taylor (1958) and Chuoke *et al* (1959) studied this in a Hele-Shaw cell and derived the condition for instabilities to develop at the moving interface. The instability in figure 1(c) is simply a special case where the original interface is stationary. Various aspects of this fingering phenomenon in a Hele-Shaw cell have been treated in subsequent papers (Taylor and Saffman 1959, Pitts 1980, McLean and Saffman 1981, Richardson 1972, 1981, Paterson 1981). If one of the plates of the cell is removed, so that a thin sheet of fluid with a free surface now flows over the remaining plate, the problem becomes much more difficult; however, it is interesting that the advancing edge of the fluid can show similar unstable fingering (Huppert 1982).

2. Basic equations

The motions we study are so slow that inertia is negligible and there is quasi-static equilibrium. The pressure drop as one crosses the interface into the liquid will be taken as $\gamma(\kappa_0 - \kappa)$, where γ is the surface tension, κ is the curvature as seen on the face of the cell (positive when the liquid is convex), and κ_0 is the (much larger) curvature in a plane normal to the cell walls. The curvature κ_0 will be taken as constant, but for the theory that follows the value of the constant is not needed. The simplest assumption, for a sufficiently small plate separation b and for a liquid that wets the plates, would be that $\kappa_0 = 2b^{-1}$; but when the interface retreats it leaves a visible thin film of liquid on the plates, whose thickness must affect κ_0 . In the experiments reported here we tried to wet the cell walls with a uniform film before each experiment. The assumption that κ_0 is constant then proves adequate, but in more accurate work it might be a source of difficulty, because $|\kappa_0| \gg |\kappa|$ and so small proportional changes in κ_0 could be large in absolute magnitude.

The plane of the cell is supposed tilted at a fixed angle β to the vertical. If we define a potential

$$\phi = P + \rho gH + \gamma\kappa_0$$

where P is the pressure, ρ is the density, g is the gravitational acceleration and H is the vertical height above a fixed level, we have within the liquid the two-dimensional vector relation in the plane of

the cell

$$\mathbf{v} = -a \text{ grad } \phi. \quad (1)$$

Here \mathbf{v} is the velocity of the liquid averaged through the thickness of the layer, and a is a constant equal to $b^2/12\eta$, where η is the viscosity (Lamb 1932). Thus, in the absence of gravity, \mathbf{v} would be proportional to the pressure gradient.

Assuming incompressibility ($\text{div } \mathbf{v} = 0$) it follows from equation (1) that ϕ is two-dimensionally harmonic:

$$\nabla^2 \phi = 0. \quad (2)$$

3. The predominant wavelength at an unstable interface

We now allow the straight interface in figure 1(b) to have a small sinusoidal perturbation and calculate whether the amplitude grows or diminishes. We can expect that surface tension will tend to stabilise perturbations of very small wavelengths, whereas those of very large wavelength, although gravitationally unstable, will only be able to grow very slowly because the slope of the interface is small. This suggests, as we now calculate, that there will be an intermediate wavelength for which the perturbation will grow at the fastest rate, and this will be the wavelength observed in experiments. We neglect end effects, on the grounds that the cell is many wavelengths wide; a narrower cell requires a separate analysis.

Consider, therefore, to start with, a semi-infinite layer and take axes $0x, 0y$ in the plane of the cell, with 0 at the unperturbed interface, $0x$ horizontal and $0y$ uphill. Let the (small) deviation of the perturbed interface from $0x$ be

$$f(x, t) = \varepsilon e^{\pi} \sin kx \quad (3)$$

ε, r and k being constants, and t being time, with the liquid lying above the curve. If we take the air pressure as constant and use this as a pressure datum, the pressure at a point just inside the liquid is $\gamma(\kappa - \kappa_0) \approx \gamma(\partial^2 f / \partial x^2 - \kappa_0)$. Hence, if the datum height for ϕ is $y = 0$,

$$\phi = \gamma \frac{\partial^2 f}{\partial x^2} + \rho g_y f$$

($g_y = g \cos \beta$). To first order this is also the value of ϕ on $y = 0$. At $y \rightarrow \infty$, where there is no disturbance, $\phi \rightarrow 0$. We shall assume, further, that the velocity of the free boundary is obtained simply by taking the normal component of \mathbf{v} at the boundary. This is an approximation because \mathbf{v} is an average velocity through the thickness derived on the assumption of a parabolic velocity profile between the plates, and near the moving boundary the flow will not be like this; in fact its details are still not well understood. With this approximation v_y , the y component of the velocity at the boundary, and

therefore at $y = 0$ to first order, must satisfy $v_y = \partial f / \partial t$. Hence, from equation (1), $\partial \phi / \partial y = -a^{-1} \partial f / \partial t$.

The solution of equation (2) that satisfies these conditions is, in terms of a constant wavenumber k_0 defined by $k_0^2 = \rho g_y / \gamma$,

$$\phi = \varepsilon \gamma (k_0^2 - k^2) e^{\pi - ky} \sin kx \quad (4)$$

with the rate constant r that appears in equation (3) given by

$$r = a \gamma k (k_0^2 - k^2). \quad (5)$$

The quantity k_0^{-1} is a capillary length appropriate to the angle the cell makes with the vertical. For $k > k_0$ (small wavelengths) r is negative, indicating exponential damping and therefore stability, while for $k < k_0$ (large wavelengths) r is positive and the disturbance is unstable, which is the behaviour expected. The wave that grows fastest (maximum r) is that for which $k = k_0 / \sqrt{3}$, a result quoted by Saffman and Taylor (1958, p. 316) and derived by Chouke *et al* (1959).

If the layer of liquid does not extend to infinity but is of finite height h , the boundary condition is $v_y = 0$ at $y = h$. The appropriate solution, in place of equation (4), is then

$\phi = \varepsilon \gamma (k_0^2 - k^2) e^{\pi} (\cosh ky - \tanh kh \sinh ky) \sin kx$
with

$$r = a \gamma k (k_0^2 - k^2) \tanh kh. \quad (6)$$

The fastest growing wave now has the wavenumber K that satisfies the transcendental equation

$$(k_0^2 - 3K^2) \sinh 2hK + 2hK(k_0^2 - K^2) = 0. \quad (7)$$

As $h \rightarrow 0$, $K \rightarrow k_0 / \sqrt{2}$ while as $h \rightarrow \infty$, $K \rightarrow k_0 / \sqrt{3}$ as previously derived. These two extreme cases are analogous to shallow and deep water dynamical waves, respectively.

4. Experimental tests of the predominant wavelength

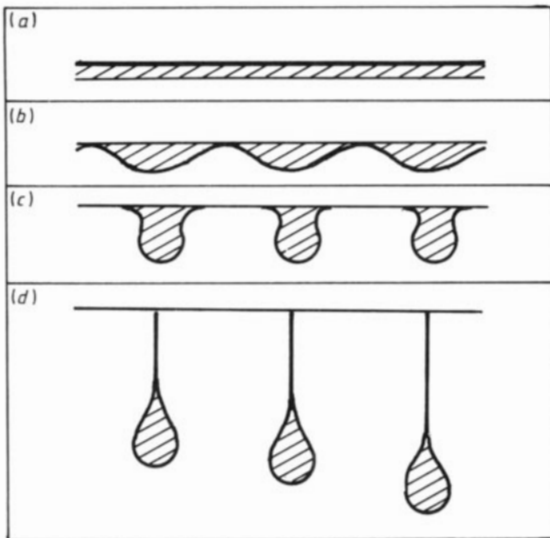
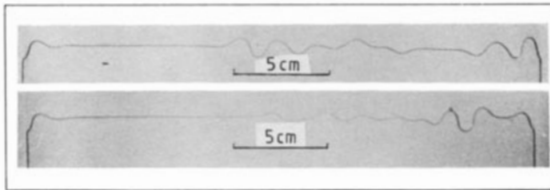
For the experiments a square-shaped cell $280\text{mm} \times 280\text{mm} \times 1.4\text{mm}$ was half-filled with oil (Shell 'Turbo T-25') and held vertically. The cell walls were first evenly wetted by very slowly turning the cell in its own plane, and then the cell was rapidly inverted as in figures 1(a) and (b). Photographs (such as those in figure 2) typically showed uneven wave trains. Their crests and troughs tended to fall into a number of groups, so that within any one group they were rather evenly spaced, but the phase jumped between groups (waves near the ends were excluded from the measurements). It was as if wave trains of limited length but rather definite wavelength were nucleated at different places with no particular phase relation between them. (Theoretically the spectrum has a peak at $k = k_0 / \sqrt{3}$ that rises exponentially with time and a bandwidth that decreases as $t^{-1/2}$.) The separate groups of

waves were used to estimate the predominant wavelength: a total of 30 estimates from 12 photographs gave a wavelength $\lambda = 20.8 \pm 0.6$ mm. This compares with a theoretical value, calculated from the formula $k = k_0/\sqrt{3}$ and measurements of the Laplace length $L = (\gamma/\rho g)^{1/2}$ of $\lambda = 20.4 \pm 1.3$ mm. The best way of handling the data needs further study, but this result suggests that the theoretical factor $1/\sqrt{3}$ is correct to within 10%. A more detailed investigation would measure the changing spectrum of the wave trains and compare it with the theoretical form.

A test of the shallow layer case, where theoretically the predominant wave has $k = k_0/\sqrt{2}$, could be made by observing a thin thread of liquid at the very top of the cell (figure 3(a)). Ripples can be seen developing in it, and as soon as their amplitude grows to the height of the layer, figure 3(b), the thread becomes a series of almost independent drops, figure 3(c) (they are actually weakly connected by the two very fine threads of liquid now

Figure 2 (Below.) Two photographs of the unstable interface, with oil above and air below. The vertical segments at the extreme right and left in each picture run down the edges of the cell.

Figure 3 (Bottom.) A shallow liquid layer at the top of the cell (a) is unstable (b), but produces drops (c) and (d) of fixed volume, which can be brought to rest by tilting the cell to reduce the effect of gravity.



left running along the top edges of the cell). These eventually develop into the roughly equally spaced pendant tethered drops, figure 3(d), whose shape we examine in sections 5 and 6. It is evident that the spacing of these drops is decided by the wavelength of the initial instability. Whether it corresponds to $k = k_0/\sqrt{2}$ has still to be tested.

Even when the cell is half full before inversion a series of roughly uniformly spaced pendant drops, originating in a residual thin thread at the top of the cell, is a notable feature of the final stage (figure 1(e)) before all the liquid reaches the lower half of the cell. As mentioned earlier, if a vertical thread in figure 1(e) breaks before the drop itself has reached the main body of the liquid, the tear-shaped drop (like A) rapidly becomes circular (like B) and continues to fall. We examine both kinds of drop theoretically in the next section.

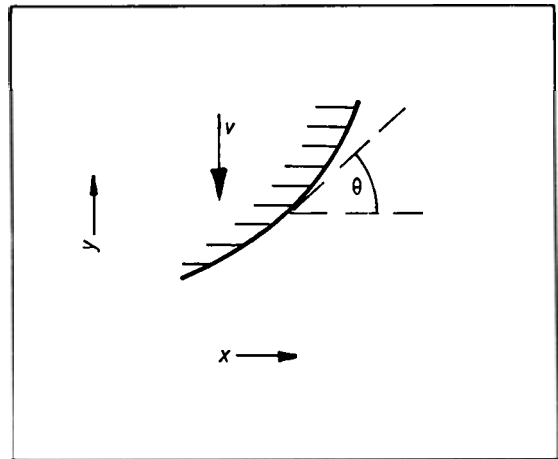
5. The shapes of falling drops and static interfaces

There is an interesting family of interface curves that correspond to uniform downward velocity v in the fluid. This includes the family of purely static shapes ($v = 0$), the falling circular drops and, to a good approximation, the falling tethered drops.

In figure 4 the fluid and the interface are assumed to be moving downwards uniformly with velocity v . The pressure, relative to the air pressure, at a point just inside the fluid is $P = \gamma(\kappa - \kappa_0)$, κ being positive as drawn. The potential ϕ , defined just as before, is at this point $\phi = \gamma\kappa + \rho g_y y$ and hence, in view of equation (1) (and noting that $v_y = -v$)

$$v = a\gamma \frac{d\kappa}{dy} + a\rho g_y \tag{8}$$

Figure 4 Coordinate system.



Thus κ is linear in y unless, exceptionally, $v = a\rho g_y$, in which case κ is constant and the interface is circular. It follows that circular drops of different radii all fall with the same velocity $a\rho g_y$ (provided their perimeters are stable). Excluding this case of circular drops, let us choose the origin for y so that $\kappa = 0$ on $y = 0$. Then, by integration

$$(a\rho g_y - v)y = -a\gamma\kappa \quad (9)$$

an equation, well known in static surface tension problems (e.g. Isenberg 1978), that describes a family of curves having curvatures proportional to height.

It is convenient to introduce as a scale length a velocity-dependent Laplace length

$$l' = l\{a\rho g_y/(a\rho g_y - v)\}^{1/2}$$

where

$$l = (\gamma/\rho g_y)^{1/2} = k_0^{-1}.$$

Thus, in the static case $v = 0$, $l' = l$. Then, writing $X = x/l'$ and $Y = y/l'$, equation (9) is simply

$$Y = -d\theta/dS \quad (10)$$

where $\tan \theta = dY/dX$ and S is the dimensionless distance along the curve. Putting $dS = dY/\sin \theta$ this equation integrates to

$$\frac{1}{2}Y^2 = c + \cos \theta \quad (11)$$

in which the constant c determines the different members of the family of curves. Evidently $c \geq -1$. The most straightforward, but crude, way of computing the curves is to return to equation (10) and use the finite difference equations

$$\left. \begin{aligned} \Delta X &= \Delta S \cos \theta \\ \Delta Y &= \Delta S \sin \theta \\ \Delta \theta &= -Y \Delta S. \end{aligned} \right\} \quad (12)$$

The integration is started at $\theta = 0$ where, from equation (11), choosing the negative square root, $Y = -\{2(c+1)\}^{1/2}$. Put $X = 0$; then, taking equal steps ΔS , the values of θ and hence of X and Y can be computed in succession along the curve. A more accurate way of computing a representative section of the curve is to use θ as a parameter, to obtain $Y(\theta)$ from equation (11), and to express $X(\theta)$ as the integral

$$X(\theta) = \int \frac{\cos \theta}{\{2(c + \cos \theta)\}^{1/2}} d\theta \quad (13a)$$

(where $Y < 0$). However, the integrand is singular if the inflexion point $\theta = \cos^{-1}(-c)$ is encountered, and then it is better to change from θ to the alternative parameter $\psi = (c + \cos \theta)^{1/2}$ with

$$X(\psi) = -\sqrt{2} \int \frac{\psi^2 - c}{\{1 - (\psi^2 - c)^2\}^{1/2}} d\psi \quad (13b)$$

($Y < 0$). This integrand is singular at $\theta = 0$. Thus, by using either form (13a) or (13b), a complete section of the curve below the X axis can be covered without singularities. The integrals in equations (13) are also expressible in terms of elliptic integrals of the first and second kinds; Bakker (1928), Wolf (1959) and Princen (1969) give further details.

Figure 5 shows how the shape of the curve changes dramatically as c takes values from -1 to $+\infty$. For $-1 < c < 1$ there are inflexions at $Y = 0$ with slope $\theta = \cos^{-1}(-c)$, and these are centres of symmetry. Note that the liquid is, by definition, always to the left of the positive S direction. The case $c = -1$ gives the straight line $Y = 0$, with $\theta \equiv 0$ (liquid above), which we have already found to be unstable to long-wave perturbations. As c increases the equilibrium curve develops meanders, until at $c = c_0 = 0.46237$ corresponding to a slope at the inflexion of $\theta = \pm 117.540^\circ$, successive waves touch one another. The part of this curve marked P in figure 5 corresponds to the tethered drop that we will consider in more detail in section 6 (the tether itself needs a different treatment). At larger values of c the curve crosses itself, but at $c = c_1 = 0.65223$ successive loops fall exactly on top of one another so that the curve becomes closed. Successive approximation is needed to find c_0 and c_1 . At $c = 1$ (exactly) the distance between successive loops becomes infinite, and, with our choice of X origin, the inflexion point, where the slope is now zero, is at infinity (an origin at the inflexion point would have given the obvious straight line solution $Y = 0$ with the liquid below). For $1 < c < \infty$ there is no longer an inflexion and the curve has two independent branches. Finally, as $c \rightarrow \infty$ the curve becomes two small remote circles with centres at heights $Y = \pm(2c)^{1/2}$ and of radius $(2c)^{-1/2}$. One circle represents a very small liquid drop and the other a very small air bubble. As static shapes ($v = 0$) one is the inverse of the other. But, if $v = a\rho g_y$, the length scale becomes infinite and we have the previously excluded case of the descending circular drop of indefinite size. A corresponding ascending circular bubble does not exist because it is not compatible with uniform downward motion of the fluid. Thus, while downward moving drops are circular, even when large, and have a velocity independent of their radius, upward moving bubbles are visibly non-circular and their velocity depends on their size. The curves in figure 5 are called undulating elastica ($c < 1$), separating elastica ($c = 1$) and nodal elastica ($c > 1$). The undulating elastica is the locus of the centre of a hyperbola rolling on a straight line, while the nodal elastica is the locus of the centre of an ellipse rolling on a straight line (Greenhill 1892, Huh 1969).

Because the curves for $c > c_0$ cross themselves they cannot describe the boundary of a semi-infinite portion of fluid. Nevertheless, parts of these

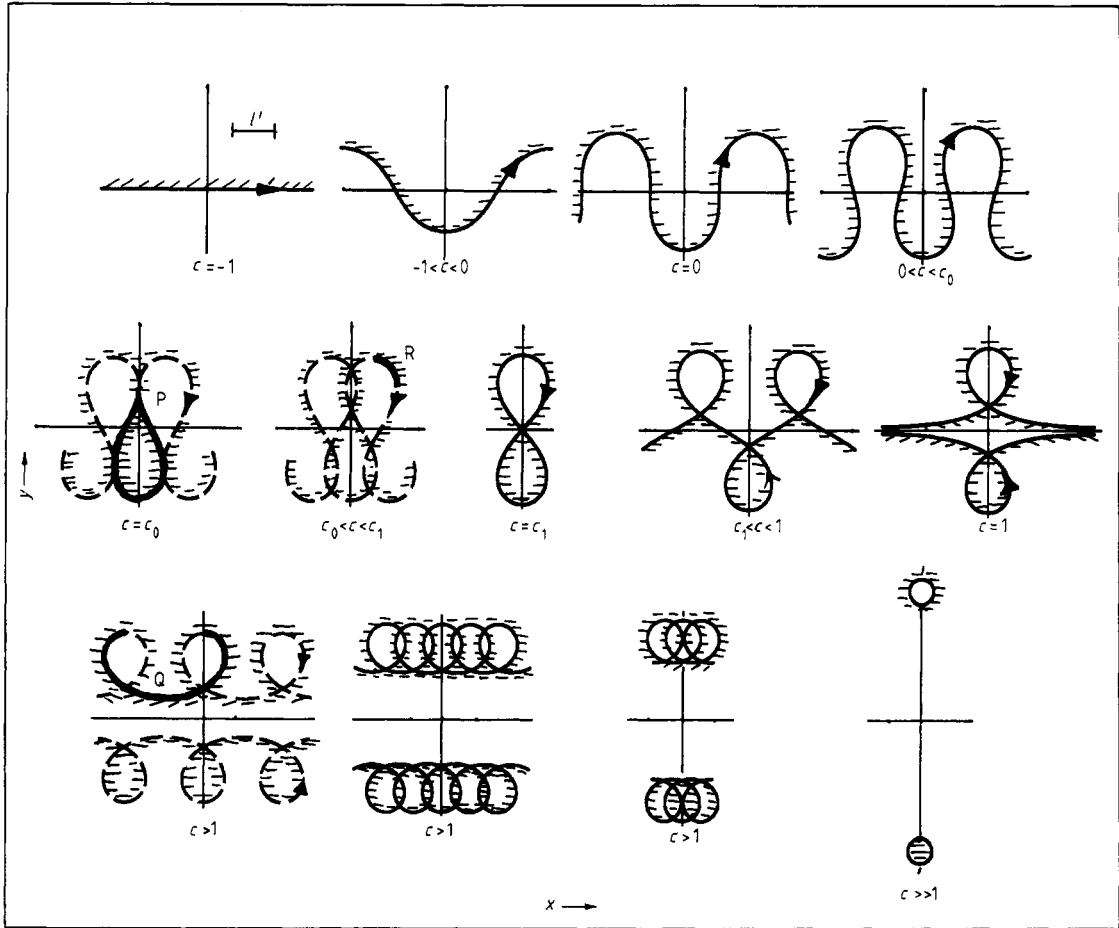


Figure 5 The one-parameter family of curves having curvature proportional to height. The successive values of the parameter c are: -1 , -0.5 , 0 , 0.25 , $c_0 = 0.46237$, 0.5 , $c_1 = 0.65223$, 0.85 , 1 , 1.1 , 1.6 , 2 , 5 . The scale unit l' , as shown in the first diagram, is the same throughout.

curves can correspond to physical configurations and are seen in experiments. For example, the section marked Q in figure 5 (lower left) represents a pendant bubble; that is, a bubble of air resting against the top edge of a nearly full cell (or, alternatively, the lower side of a bubble of air floating on the upper free surface of a part-filled cell). On the other hand, the mirror-image sessile drop shape given by the lower branch is not realised in our experiments because the liquid wets the boundary of the cell. A triangular-shaped portion of fluid in an upper corner of the cell, such as R , is another example.

The series of undulatory shapes with $-1 < c < c_0$ are not seen in experiments as the lower boundary of a semi-infinite portion of fluid, presumably because they are then unstable. This can be understood as follows. The wavelength of the static meanders, when c just exceeds -1 , is $2\pi l$, i.e. the

wavenumber is l^{-1} , which happens to be precisely equal to the critical wavenumber k_0 that we found dividing stable from unstable sinusoidal perturbations (equation (5)). The repeat distances of the static curves with $-1 < c < c_0$ are all less than $2\pi l$. Consider then a family of undulations of wavelength slightly less than $2\pi l$, of fixed phase but of adjustable amplitude A . The state $A = 0$ is in equilibrium and equation (5) shows that it is stable with respect to changes in A . However, we now know that two small values of A on either side of zero, in fact $A = \pm l\{2(c+1)\}^{1/2}$, also give equilibrium (they are the static curve just described for c near -1 and its mirror image in $y = 0$). By continuity of the potential energy curve these flanking equilibria must necessarily be unstable. As $c \rightarrow -1$ from above the three equilibria approach one another and the potential energy curve at $A = 0$ becomes quartic rather than parabolic (as we could have

expected from the earlier perturbation analysis).

Although these shapes with $-1 < c < c_0$ are unstable when taken as the boundary of a semi-infinite portion of the fluid, they can nevertheless be found stably in static experiments by starting with a shallow layer at the top edge of the cell as in figure 3. After stage 3(b) an almost fixed volume is trapped in each loop. If the cell is now tilted to reduce the component of gravity, an angle can be found at which the drops no longer grow. The shape is then a part of one of the statical equilibrium curves with $-1 < c < c_0$. The fixing of the volume evidently stabilises the shape. Boucher and Jones (1983) have discussed the closely-related problem of the stability of two-dimensional pendant drops, not in a Hele-Shaw cell.

6. Tethered drops

The tethered drops in the experiments have a variety of sizes, but the analysis in section 5 shows that, provided the assumption of uniform v is valid, they all have the same universal shape, namely that corresponding to $c = c_0$ (although the tether can have any length). This is possible because v enters the length scale. To represent the size of a drop let us choose its maximum width w . By calculation $w = 1.2859l'$, and so from the definition of the length scale l' we find

$$v = apg_v \left(1 - 1.6536 \frac{l'^2}{w^2} \right) \quad (14)$$

as the relation between velocity and size. Of course, a lower limit to the permissible w is set by the separation of the plates of the cell. As $w \rightarrow \infty$, $v \rightarrow apg_v$, which we have already noted as the velocity of circular drops. Thus, as the tethered drop becomes larger, its shape stays the same but its velocity approaches that of a circular drop (of any size). However, this result must be qualified by remarking that the results of section 3, when extended to $v \neq 0$, suggest that above a certain size the shape of a tethered drop will be unstable to small perturbations.

To study the effect of tilting the cell through an angle β to the vertical we write equation (14) in terms of the unmodified Laplace length $L = (\gamma/\rho g)^{1/2}$, thus

$$v = apg(\cos \beta - 1.6536 L^2/w^2). \quad (15)$$

This shows that a tethered drop of given w can be brought to rest by making β such that

$$\cos \beta = 1.6536 \frac{L^2}{w^2}. \quad (16)$$

In this state the component down the slope of the weight of the drop is just balanced by the surface tension of the tether. Further tilting causes the drop

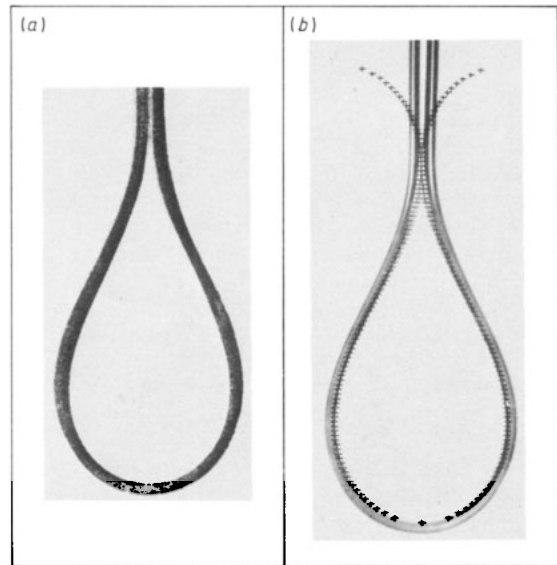


Figure 6 (a), Five superimposed photographs of tethered drops of different sizes but with the enlargements adjusted so that the images coincide. The shape is independent of size. (b), A photograph of a tethered drop compared with the theoretical shape (crosses). Width = 5.2 mm.

to be pulled upwards. In a cell of given tilt β , falling tethered drops should all have widths greater than that given by equation (16).

An experimental test of equation (14) was made by first measuring the velocity of free circular drops in a vertical cell. The fact that the drops are circular, in spite of the lack of symmetry implied by their motion, is a sensitive test of the assumption that κ_0 is constant. The velocity measurements gave $apg_v = apg = 3.38 \pm 0.06 \text{ mm s}^{-1}$. Then v was plotted against w^{-2} for tethered drops. Most of the velocities of the tethered drops were within about 2% of those expected from equation (14), but a few moved 20–30% faster. After the oil has reached the bottom of the cell (figure 1(a)) a thin film of oil remains on the walls and the visible unevennesses in its thickness are observed to affect the course of the later sequence (figures 1(b)–(f)). This, and unwanted variations in the spacing between the cell walls, are probably the cause of the deviant results.

Photographs of falling tethered drops showed that, although their shapes were very close to the calculated one, nevertheless there were small systematic deviations. The angle θ at the inflexion was systematically high, between 120° and 124° compared with the theoretical value of 117.540° . The explanation is almost certainly in the assumption that v is uniform within the falling drop. This ignores the small amount of fluid left behind in the tether as the drop descends, which must mean that v changes rapidly from the bulk value to nearly

zero over a small distance near the neck of the drop.

However, the shape analysis ought to apply very accurately if a drop is brought to rest by tilting the cell. Figure 6(a) shows five superimposed photographs of stationary tethered drops with widths ranging from 5.2 to 6.8 mm, the enlargements being adjusted for the best registration; the shapes are indistinguishable from each other, as predicted. Figure 6(b) compares the shape of one of these with the theoretical curve. The fit is excellent, even at the top where the apparent slight discrepancy is caused by the fainter part of the inside of the meniscus not being reproduced in the printing. Full accounts of the experiments are given by Lean (1983) and Wright (1983).

Acknowledgments

We thank Dr E A Boucher and Dr D H Peregrine for directing us to relevant literature, and Professor M V Berry for helpful discussion.

References

- Bakker G 1928 *Handbuch der Experimentalphysik* vol 6 *Kapillarität und Oberflächenspannung* (Leipzig: Akademische Verlagsgesellschaft) pp 83-7
- Boucher E A and Jones T G J 1983 *J. Colloid and Interface Science* **91** 301-6
- Chuoque R L, van Meurs P and van der Poel C 1959 *Trans. AIME* **216** 188-94.
- Greenhill A G 1892 *The Applications of Elliptic Functions* (London: Macmillan) p. 190
- Hele-Shaw H J S 1898a *Trans. Inst. Nav. Arch.* **40** 21-46
- 1898b *Nature* **58** 34-6
- Huh C 1969 *Capillary Hydrodynamics* PhD Thesis, University of Minnesota, University Microfilms International, London, England (1977)
- Huppert H E 1982 *Nature* **300** 427-9
- Isenberg C 1978 *The Science of Soap Films and Soap Bubbles* (Clevedon: Tieto) p. 115
- Lamb H 1932 *Hydrodynamics* 6th edn (Cambridge: Cambridge University Press) §330
- Lean H W 1983 Unpublished: Project 14, in Physics Library, University of Bristol
- McLean J W and Saffman P G 1981 *J. Fluid Mech.* **102** 455-69
- Paterson L 1981 *J. Fluid Mech.* **113** 513-29
- Pitts E 1980 *J. Fluid Mech.* **97** 53-64
- Princen H M 1969 *Surface and Colloid Science* ed. E Matijević **2** 1-84
- Richardson S 1972 *J. Fluid Mech.* **56** 609-18
- 1981 *J. Fluid Mech.* **102** 263-78
- Saffman P G and Taylor G I 1958 *Proc. R. Soc. A* **245** 312-29
- Taylor G I and Saffman P G 1959 *Quarterly Journ. Mech. Appl. Math.* **12** 265-79
- Wolf K L 1959 *Physik und Chemie der Grenzflächen* vol. 2 (Berlin: Springer-Verlag) pp 41-9
- Wright A N 1983 Unpublished: Project 14, in Physics Library, University of Bristol